A New Two-Way Ensemble Prediction for Infectious Diseases

Yingjie Zhao, Jianping Huang, Rui Wang, Han Li, Wei Yan, Xinbo Lian, and Zihan Hao

***Abstract*—Infectious diseases pose a persistent global health threat, making accurate forecasting essential for effective response. A deep understanding of their underlying mechanisms and the role of environmental factors is crucial to improving predictive models. In this study, we first investigate the relationship between key meteorological variables, including average temperature, relative humidity, PM2.5, and PM10 and the progression of infectious diseases, using COVID-19 data from Beijing and Shanghai as a representative case. A generalized additive model (GAM) is employed to determine the driven meteorological factors that affected the development of infectious diseases in general. Based on this analysis, we incorporate the identified meteorological variables into a modified susceptible–exposed–infected–recovered (SEIR) model. Then, further integrated this model into a novel two-way ensemble prediction (TEP) framework. This integrated method captures temporal and spatial dynamics of disease transmission. The proposed method demonstrated a significant improvement in prediction accuracy compared to traditional epidemiological models. This two-way integrated modeling framework offers a practical and rapid response to epidemic forecasting, providing valuable insights for future pandemic predictions, especially in regions with limited data on human mobility.**

***Index Terms*—Generalized additive model (GAM), infectious diseases, modified susceptible–exposed–infected–recovered (SEIR) model, two-way ensemble prediction (TEP).**

I. Introduction

THE investigation into analyzing the underlying mechanism of the spread of infectious diseases is of great interest to many researchers, forecasting epidemic trajectories has also been an important area of research in recent years. Although COVID-19 has been a focal point, the insights from these studies are broadly applicable to a range of infectious diseases, with plenty of methodologies and models being proposed to enhance the accuracy of such predictions [1], [2], [3], [4], [5], [6]. Among them, the most classic and frequently used models are susceptible–infected–recovered (SIR) and susceptible–exposed–infected–recovered (SEIR) models. These models, introduced over a century ago, have been widely utilized to predict the development of various infectious diseases, including COVID-19 [7], [8], [9]. It is true that they had good performances back in that time, but they started to show some limitations when applied to predicting the trend of infectious diseases occurred in recent years. A primary shortcoming of compartmental models such as the SIR and SEIR models lies in their inability to adequately account for the dynamics of human mobility [10]. Human movement plays an important role in virus transmission, as individuals carry the virus across geographic regions, leading to spatial and temporal variations in disease spread. These mobility-driven dynamics are critical for understanding the spread of infectious diseases across regions but are insufficiently captured by traditional compartmental models. This oversight in the models leads to a deficit in accurately depicting the evolution of infectious diseases, particularly in contemporary scenarios where human mobility is notably frequent.

Apart from the limitations of the models themselves, the effects the climate factors have on the development of infectious diseases have always been a prominent area of research throughout a long period of time. Environmental factors, including temperature, humidity, and precipitation, have long been recognized as significant contributors in influencing the transmission and spread of infectious diseases [11], [12], [13]. Several studies have demonstrated the link between climate variables and the seasonality of diseases such as influenza, malaria, and respiratory infections. The impact of weather on disease transmission is particularly evident in temperate climates, where seasonal fluctuations coincide with peaks in disease incidence [14]. As a result, understanding the relationship between meteorological conditions and infectious diseases has become a crucial area of research, especially in the context of global public health. As a climate-sensitive disease, COVID-19 shows an obvious seasonality in higher latitude regions [15]. Besides, the optimal temperature for the spread of COVID-19 is between 5 °C and 15 °C [16]. Apart from the analysis

Received 26 April 2025; revised 13 November 2025; accepted 2 December 2025. Date of publication 26 December 2025; date of current version 2 October 2026. This work was supported in part by the National Key Research and Development Program of China under Grant 2023YFC3503400, in part by the R&D Program of Guangzhou Laboratory under Grant SRPG22-007, in part by Gansu Province Intellectual Property Project under Grant 22ZSCQD02, in part by the Youth Program of the National Natural Science Foundation of China under Grant 42505019, in part by Gansu Province Science and Technology Plan Project Youth Science and Technology Fund under grant 25JRRA707, and in part by China Postdoctoral Science Foundation under Grant 2025M770301. *(Corresponding author: Jianping Huang.)*

Yingjie Zhao, Rui Wang, Han Li, Wei Yan, Xinbo Lian, and Zihan Hao are with the College of Atmospheric Sciences, Lanzhou University, Lanzhou 730000, China (e-mail: zhaoyj22@lzu.edu.cn; wangr22@lzu.edu.cn; lihan19@lzu.edu.cn; yanw2018@lzu.edu.cn; lianxb19@lzu.edu.cn; haozh19@lzu.edu.cn).

Jianping Huang is with the College of Atmospheric Sciences, Lanzhou University, Lanzhou 730000, China, and also with the Collaborative Innovation Centre for Western Ecological Safety (CIWES), Lanzhou University, Lanzhou 730000, China (e-mail: hjp@lzu.edu.cn).

Digital Object Identifier 10.1109/TCSS.2025.3640950

2329-924X © 2025 IEEE. All rights reserved, including rights for text and data mining, and training of artificial intelligence and similar technologies. Personal use is permitted, but republication/redistribution requires IEEE permission. See https://www.ieee.org/publications/rights/index.html for more information.

Authorized licensed use limited to: Lanzhou University. Downloaded on November 10,2026 at 10:13:19 UTC from IEEE Xplore. Restrictions apply.

on the relationship between temperature and COVID-19, other environmental factors have been investigated frequently. Some researchers pointed out that the clinical manifestation of patients will be boosted after the contact with particulate matters [17], [18]. In addition, a study conducted by [19] showed that SARS-CoV-2 would be viable in aerosols, which further indicated the fact that the aerosol transmission of COVID-19 is possible.

In addition, the feature of the development of infectious diseases is another important factor. Human mobility is a key driver in the transmission and spatial dynamics of infectious diseases [20], [21], [22], [23]. The dramatic rise in global population and advances in transportation have intensified human interactions, facilitating both local and long-distance spread of pathogens [24]. Air travel, for instance, has played a pivotal role in past outbreaks such as SARS, MERS, Ebola, and influenza [25]. Numerous studies have demonstrated that mobility, which ranges from intra-city to international, contributes significantly to disease propagation [26], [27], [28], [29], [30]. Therefore, human mobility played an important role in spreading the virus, especially during the COVID-19 pandemic, as a study pointed out that intra-city mobility and inter-city mobility have averagely contributed to 57.35% and 15.18% increase in COVID-19 confirmed cases in China [22], with modeling suggesting that the absence of lockdowns could have led to over 100% more confirmed cases outside Hubei province [31]. Furthermore, when the restriction measures, such as lockdown, are implemented, the increase rate of COVID-19 cases declined considerably [32]. These findings highlight the complexity of predicting infectious disease dynamics in densely populated megacities, where human mobility patterns significantly influence epidemic trends.

In order to tackle the above-mentioned problem, a new approach named multisource dynamic ensemble prediction (MDEP) method has been proposed by Huang et al. [33], which aims to simulate the multiwave development of infectious diseases caused by human mobility and improve the accuracy of the predictions. This approach combines a modified SEIR model, which incorporates temperature and relative humidity variables, with ensemble forecasting techniques commonly used in meteorological predictions. The aim of this model is to overcome the defects of SIR and SEIR, which refers to the incapability of depicting the multiwave development of epidemics, by assembling the prediction results from each wave dynamically to get the final integrated results [33]. According to this study, the MDEP method has successfully improved the prediction accuracy to around 90%. However, the MDEP method only integrated the results over time, and it did not take the spatial distribution into consideration. Due to the different development levels of each district in a city, the development of infectious diseases would show heterogeneous trends. Therefore, it is more reasonable to include the feature of spatial distribution in the existing MDEP method. Some seasonal prediction studies on East Asia and High Mountain Asia show that treating spatial and temporal ability jointly can unlock additional predictability beyond space-only or time-only approaches [34], [35].

In this study, we aim to advance infectious disease forecasting by integrating environmental variables into a novel predictive framework. Using COVID-19 as a case study, we first used the generalized additive model (GAM) to analyze the relationship between environmental factors, namely average temperature, relative humidity, $PM_{2.5}$, and PM_{10}, and the disease dynamics in two major Chinese cities, as well as their contributions to the spread of COVID-19, and integrate these influential variables into an enhanced modified SEIR framework, explicitly accounting for the impact of meteorological changes [4], and then incorporate with the proposed two-way ensemble prediction (TEP) method, an enhanced version of MDEP that aggregates data temporally within each region and then spatially across regions to approximate mobility-induced multiwave dynamics without explicit mobility data. This interpretable design differs from prior ensemble models that require external mobility data or large machine learning datasets, and the accuracy has been improved in two megacities, namely, Beijing and Shanghai. Although COVID-19 provides the empirical basis for this study, the methodology is designed to be broadly applicable to a range of infectious diseases, highlighting the importance of environmental context in epidemic modeling and public health planning.

II. Materials and Methods

A. GAM

GAM is employed in this study to analyze the relationship between environmental variables and COVID-19 daily cases. GAM is widely used in the fields of environmental and epidemiological research due to its flexibility and ability to capture and depict the nonlinear relationships between response variables and explanatory variables [36], [37]. This feature makes GAMs particularly useful when investigating the impacts of environmental factors, such as meteorological conditions, on the incidence of infectious diseases. The use of smooth functions for predictors in GAMs enables the model to adjust to fluctuations in data that may not follow linear trends, and the GAM is used solely to estimate smooth exposure-response functions for meteorological covariates, which means it is not used to directly predict the infections. The estimated effects serve only to calibrate the time-varying transmission rate in the later modified SEIR model. This design minimizes overfitting and avoids conflicting statistical associations with mechanistic transmission dynamics. The model used in this study is described as follows:

$$\begin{aligned} y_{dt} &= \text{Poisson}(\mu_{dt}) \\ \log(\mu_{dt}) &= \log\left(\text{popu}_d\right) + \beta_0 + \sum_{j=1}^{n} f_j(x_{j,dt}) \end{aligned} \tag{1}$$

where y_{dt} denotes the observed number of cases in region d on day t, and popu_d represents the population size in region d. $f_j(\cdot)$ is smooth functions of the environmental covariates $x_{j,dt}$, namely average temperature, relative humidity, $PM_{2.5}$,

Authorized licensed use limited to: Lanzhou University. Downloaded on November 10,2026 at 10:13:19 UTC from IEEE Xplore. Restrictions apply.

and PM_{10}, $popu_d$ is the offset of population in different regions d, and β_0 is the intercept. Equation (1) is equivalent to modeling the log incidence rate

$$\log\left(\frac{\mu_{dt}}{\text{popu}_d}\right) = \beta_0 + \sum_{j=1}^{n} f_j(x_{j,dt}). \tag{2}$$

So, all smooth effects are interpreted as multiplicative effects (rate ratios) on incidence rather than on raw counts. This formulation removes spurious correlation between total cases and population size by conditioning on exposure through the offsets.

B. Spatial Weighted K-Means Method

K-means and spatial weighted K-means are commonly used clustering algorithms employed in spatial data analysis, each serving distinct purposes based on the nature of the data. The traditional K-means algorithm partitions n data points into k clusters by minimizing the within-cluster sum of squared Euclidean distances, as defined by the objective function [38]

$$J = \sum_{i=1}^{k}\sum_{j=1}^{n_i} ||x_j - \mu_i||^2 \tag{3}$$

where x_j represents the data points, μ_i denotes the cluster centroids, and n_i is the number of points in cluster i. While effective for general clustering tasks, K-means does not account for spatial dependencies or the inherent geographic structure of the data.

In contrast, spatial weighted K-means extends the traditional approach by incorporating spatial weights into the clustering process, thereby considering the spatial relationships between data points. In this study, we use spatial weighted K-means which incorporate the epidemic data and meteorological data to group districts. The modified objective function can be expressed as

$$J_{swk} = \sum_{i=1}^{K}\sum_{j\in C_i} \omega_{ji}||M^{\frac{1}{2}}(x_j - \mu_i)||^2 \tag{4}$$

where x_j is the feature vector for district j, μ_i is the centroid of cluster C_i, ω_{ji} is a spatial weight linking district j to cluster i, and M is a feature-weight matrix. It should be noted that each region's feature vector (x_j) concatenates epidemic and population information, and the formation of x_j is as follows:

$$x_j = [i_{j,t}, \ldots, i_{j,t_T}, \log(\text{popu}_j)]^T \tag{4a}$$

where $i_{j,t}$ represents region-level epidemic cases over the study window $t_1 : t_T$, and $\log(\text{popu}_j)$ represents the population size in each region. As for centroid μ_i, the calculation equation is

$$\mu_i = \frac{\sum_{j\in C_i}\omega_{ji}x_j}{\sum_{j\in C_i}\omega_{ji}}. \tag{4b}$$

This formulation ensures that spatially proximate regions with similar trajectories and population scales are more likely to be grouped together, thus, preserving the spatial autocorrelation.

When analyzing the distribution of an epidemic, spatial weighted K-means is often preferred over the standard K-means due to its ability to account for spatial dependencies and regional heterogeneities. Epidemic data exhibit spatial patterns influenced by factors such as population density, mobility, and environmental conditions. By integrating spatial weights, spatial-weighted K-means can more accurately capture these localized variations, leading to more meaningful and interpretable clusters that reflect the true spatial dynamics of the epidemic spread. Moreover, other spatial analysis methods, such as Moran's I and LISA are univariate autocorrelation diagnostics and do not accommodate multivariate inputs [39], whereas spatial weighted K-means jointly use each district epidemic trajectory and population to produce spatially coherent risk strata. Importantly, this clustering is used only to stabilize small-area inference and organize aggregation, which means it does not enter the prediction model.

C. Modified SEIR Model

This study utilizes the SMDEP method, which builds on the modified SEIR model and ensemble forecasting techniques commonly used in weather prediction [40]. The modified SEIR model extends the classic SEIR framework by incorporating additional compartments: P (protected), Q (quarantined), and D (dead), allowing for a more comprehensive representation of disease dynamics. The model is governed by the following system of differential equations [41], [42]:

$$\frac{dS_d(t)}{dt} = -\frac{\beta_d I_d(t) S_d(t)}{N_d} - \alpha_d S_d(t) \tag{5}$$

$$\frac{dP_d(t)}{dt} = \alpha_d S_d(t) \tag{6}$$

$$\frac{dE_d(t)}{dt} = \frac{\beta_d I_d(t) S_d(t)}{N_d} - \gamma_d E_d(t) \tag{7}$$

$$\frac{dI_d(t)}{dt} = \gamma_d E_d(t) - \delta_d I_d(t) \tag{8}$$

$$\frac{dQ_d(t)}{dt} = \delta_d I_d(t) - \lambda_d Q_d(t) - \kappa_d Q_d(t) \tag{9}$$

$$\frac{dR_d(t)}{dt} = \lambda_d Q_d(t) \tag{10}$$

$$\frac{dD_d(t)}{dt} = \kappa_d Q_d(t). \tag{11}$$

In this epidemiological model, we define the total population in each region d as N_d, where $N_d = S_d + P_d + E_d + I_d + Q_d + D_d + R_d$. The model incorporates several key parameters: the protection rate α_d, which quantifies the rate at which individuals transition to a protected phase; and the rate β_d dictates the rate at which susceptible individuals become exposed. After the latent time $(1/\gamma_d)$, the exposed population will become infectious, among whom a certain part of the infected people will be quarantined at the rate δ_d. In addition, the rate λ_d and κ_d are recovery and death rates, respectively. It is important to note that all these parameters are positive values, except the protection rate α_d where a positive value indicates a transition from the susceptible to the protected phase, whereas a negative value indicates a return to the susceptible population. In addition, the model introduces a nuanced approach to the transmission rate β_d, expressed as

$$\beta_r = \beta_{0r} + \beta_{1r}F(T_{2mr}) + \beta_{2r}F(\text{RH}_{2mr}) \tag{12}$$

Authorized licensed use limited to: Lanzhou University. Downloaded on November 10,2026 at 10:13:19 UTC from IEEE Xplore. Restrictions apply.

where β_{0r} represents the baseline transmission rate in region d, while β_{1r} and β_{2r} are coefficients that modulate the influence of environmental factors on transmission, specifically temperature and humidity, respectively. $F(T_{2mr})$ and $F(RH_{2mr})$ are probability distribution functions that describe the effects of temperature in region d (T_{2mr} measured 2 m above ground level) and relative humidity in region d (RH_{2mr} measured 2 m above ground level) on disease transmission, as established by [4]. Equation (12) specifies the SEIR transmission rate β_r with temperature- and humidity-based modulation, whose coefficients are estimated within the SEIR model. All parameters in (12) are fitted separately for each risk level region, and particular matters are deliberately excluded from β_r to maintain simplicity and limit overfitting.

The underlying mechanism of the modified SEIR model involves tracking the flow of individuals between compartments over time using rates that represent disease dynamics. The model relies on initial conditions derived from epidemic data, including the number of susceptible, exposed, infected, and recovered individuals. By solving the system of differential equations, it predicts how the infection will progress. Since it is difficult to obtain exact coefficients from real-world data, we employed an inverse coefficient method, commonly used in weather and climate predictions, to estimate these values. Specifically, we assigned initial coefficient values based on relevant literature, and then applied optimization algorithms, such as least squares, along with real-time epidemic data to adjust and refine these coefficients. The optimized coefficients are then fed back into the model to improve the accuracy of epidemic predictions.

D. TEP Method

To enhance the forecasting performance of the modified SEIR model, we developed a TEP framework, which builds upon the existing MDEP method. The MDEP approach dynamically integrates epidemic predictions by segmenting the outbreak into multiple waves and updating forecasts as new data become available, thereby addressing the limitations of incomplete initial conditions and evolving transmission dynamics [33], [40]. Each wave is predicted dynamically as the epidemic evolves, using the equation [33]

$$Y = \sum_{i=0}^{j} y_{i,j} \tag{13}$$

where i represents the wave number (e.g., 0 for the initial wave), and j represents the days within each wave. Predictions for each wave are added to previous ones, forming an integrated forecast over time. Here is an explanation in terms of the identification of new waves: as the epidemic progresses, new sources of infection can emerge, each generating its own transmission chain, thus triggering a new wave. Consequently, the epidemic typically exhibits multiple waves, which are conceptually equivalent to different stages, the definition of a new wave is determined by the monotonic behavior of the epidemic data. Monotonic increase in the data indicates the epidemic is in an upward phase, while a monotonic decrease suggests the current wave is approaching its end. When the data reaches a local minimum, it signifies the conclusion of the current wave and the potential onset of a subsequent wave.

To incorporate spatial heterogeneity, we extend MDEP into a two-dimensional ensemble framework—referred to as the TEP method. In the TEP framework, we linked environmental covariates to transmission rate, where the calibration step preserves mechanical structure while limiting overfitting. Specifically, we first estimate smooth exposure-response functions for average temperature, relative humidity, $\mathrm{PM}_{2.5}$, and PM_{10} using a GAM, and these functions are used solely to modulate the time varying transmission rate in the modified SEIR model and are not used for prediction or in the ensemble process. We then fit the modified SEIR model separately for each risk region with location-specific parameters to capture epidemiological heterogeneity and ensemble across epidemic waves with each risk region, using MDEP method, and aggregate different risk region trajectories to the city level. This spatial integration approximates cross-region infection pressure by summing heterogeneous local dynamics, while spatial weighted K-means is used to only stabilize small-area inference and organize aggregation, which means it does not impose explicit inter-region transmission terms. Because real-time mobility data was unavailable, we did not include the cross-region flow terms, instead, the design maintains mechanistic interpretability and yields robust prediction under data-scarce conditions. Moreover, the TEP method is used as the primary method, and the coefficients for the epidemics in different locations are obtained through the inverse coefficient method to generate location-specific prediction results. It is important to know that the values of these coefficients vary across models, reflecting the differences in how COVID-19 progresses in each region The equations of TEP are as follows:

$$y_m = \sum_{i=0}^{j} y_{i,j} \tag{14}$$

$$Y = \sum_{m=1}^{n} y_m \tag{15}$$

where Y represents the final integrated forecast, m is the district number, and n is the total number of districts. This approach provides a comprehensive and updated prediction of the epidemic's progression, both temporally and spatially. The complete process is illustrated in Fig. 1.

E. The Complete Workflow of TEP Work Frame

According to the above-mentioned methods, we integrate them together and provide a demonstration of the complete TEP workflow, so that the connection between each method or model can be clear. Overall, the complete workflow contains three stages, namely impulse, prediction process, and output. Specifically, the inputs of TEP workflow involve district-level daily cases for Beijing and Shanghai, meteorological data (average temperature, relative humidity, $\mathrm{PM}_{2.5}$, and PM_{10}), and district-level population. The prediction process includes four main steps. The first step is to analyze the effects of meteorological

Authorized licensed use limited to: Lanzhou University. Downloaded on November 10,2026 at 10:13:19 UTC from IEEE Xplore. Restrictions apply.

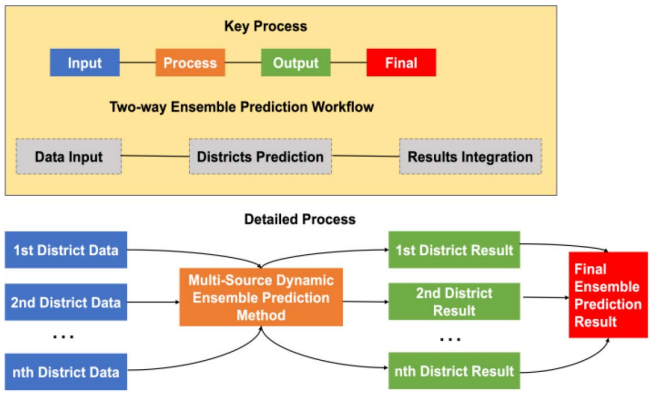


Fig. 1. Flow chart of TEP method. The upper panel shows the key stages of TEP method and the overview of workflow of TEP method, while the bottom panel shows the detailed workflow of TEP method.

covariates on the development of COVID-19 using GAM. We fit GAM to estimate smooth exposure-response functions and lags for temperature, humidity, and particulate matter. These smooth functions are used only to calibrate the transmission rate in the mechanistic model, which, in particular, refers to average temperature and relative humidity, since the effects of particulate matter are not as significant as former variables. It should be noted that the GAM does not generate predictions or enter the ensemble stage. In the second step, the district-level daily case data is fit into a modified SEIR model with the local-specific parameters and time-varying transmission rate calibrated by temperature and humidity from step 1. The third step is to use the MDEP method to integrate the predictions temporally. Before the temporal ensemble step, the district-level cases will be grouped into different risk regions, using spatial-weighted K-means, which is only used to describe heterogeneity and stabilize small-area inference. In this step, the epidemic waves are predicated sequentially and dynamically combined to form a single risk-level trajectory. Finally, the risk-level region predictions are summed to produce city-level predictions, approximating inter-region diffusion without requiring real-time mobility data, and this step is known as TEP. The outputs of the TEP workflow are daily predicted cases and cumulative predicted cases, and the accuracy assessed with mean absolute error (MAE), root mean squared error (RMSE), and R^2.

F. Methods for Calculating the Accuracy Rates

In this study, we employed three different metrics to assess the performance of each prediction method, namely MAE, RMSE, the coefficient of determination (R^2), and Mean Absolute Percentage Error (MAPE). MAE is calculated as the average of the absolute differences between predicted values $\hat{y}_i$ and actual values y_i, expressed by the equation

$$\mathrm{MAE} = \frac{1}{n}\sum_{i=1}^{n}|y_i - \hat{y}_i|. \tag{16}$$

On the other hand, RMSE is the square root of the mean of the squared differences, formulated as

$$\mathrm{RMSE} = \sqrt{\frac{1}{n}\sum_{i=1}^{n}(yi - \hat{y}_i)^2}. \tag{17}$$

It penalizes larger errors more heavily than MAE. The R^2metric measures the proportion of variance in the dependent variable that is predictable from the independent variables, and is defined by

$$R^2 = 1 - \frac{\sum_{i=1}^{n}(yi - \hat{y}_i)^2}{\sum_{i=1}^{n}(yi - \overline{y})^2}. \tag{18}$$

Because TEP produces point prediction, we quantify predictive uncertainty using an empirical residual approach. For each date t, we compute residuals $e_t = y_t - \hat{y}_t$ from the evaluation period. Predictive interval (PI) at nominal level p is obtained by shifting the point forecast by the empirical residual quantiles

$$\mathrm{PI}_p(t) = \left[\hat{y}_t + q_e\left(\frac{1-p}{2}\right), \hat{y}_t q_e\left(1 - \frac{1-p}{2}\right)\right]. \tag{19}$$

For each risk-level wave segment, we fit model parameters $\theta = (\alpha_d, \beta_{0r}, \beta_{1r}, \beta_{2r}, \gamma_d, \delta_d, \lambda_d, \kappa_d)$ to daily cases, and simulate stochastic daily transitions in a modified SEIR model with a calibrated transmission rate $\beta_r = \beta_{0r} + \beta_{1r}F(T_{2mr}) + \beta_{2r}F(\mathrm{RH}_{2mr})$. Then, wave-level trajectories were integrated temporally within each district, and this process is known as MDEP and subsequently summed across different risk-level regions to obtain city-level TEP prediction results. The ensemble results will then be summarized by daily predictive quantiles and reported empirical PI coverage against the corresponding observations.

Together, these metrics provide a comprehensive assessment of a method's accuracy and explanatory power. As for cumulative results, we use the following equation:

$$\mathrm{MAPE}_m = \frac{100}{T}\sum_{t\in\tau}\left|\frac{\hat{y}_{m,t} - y_t}{y_t}\right|, \tau = \{t\colon y_t > 0\} \tag{20}$$

where y_t represents the observed cumulative cases on day t, and $\hat{y}_{m,t}$ represents the predicted cumulative cases from model m.

G. Data Sources

The data of COVID-19 confirmed (N_C) cases was collected from Shanghai Municipal Health Commission (https://wsjkw.sh.gov.cn/yqtb/index.html) from 5 March 2022 to 31 May 2022. In addition, daily epidemic data for COVID-19 in Beijing were obtained from the National Health Commission of the People's Republic of China (http://www.nhc.gov.cn/xcs/yqtb/list_gzbd.shtml). The time period for COVID-19 data in Beijing was from 22 April 2022 to 30 June 2022. All the data are updated on a daily basis and grouped district-wise. The meteorological data, namely average temperature, relative humidity, $\mathrm{PM}_{2.5}$, and PM_{10} were collected from the website of China Meteorological Administration (http://data.cma.cn). All the COVID-19 data counts used in the manuscript are raw counts, so that it can reflect the real development of COVID-19 in different regions, thus, providing reliable and robust prediction results.

Authorized licensed use limited to: Lanzhou University. Downloaded on November 10,2026 at 10:13:19 UTC from IEEE Xplore. Restrictions apply.

III. Results

A. Meteorological Effects on COVID-19 Epidemic

Meteorological factors are well-known to have delayed effects on the incidence of infectious diseases. Therefore, in this research, we used the lagged data on the meteorological variables, including average temperature, relative humidity, $PM_{2.5}$, and PM_{10}, to analyze their effects on COVID-19 daily counts in Beijing and Shanghai, respectively. To determine the optimal lag period, we tested a range of 1–14 days for each variable in the GAM, as the most significant positive association between temperature and humidity and COVID-19 incidence was found from 3 to 11 lagged days [43]. The results indicated that the highest variance explanation was achieved with a lag of 3 days on average temperature and 5 days on relative humidity, $PM_{2.5}$, and PM_{10} for Beijing, and 7 days on average temperature and 8 days on relative humidity, and 4 days on $PM_{2.5}$ and PM_{10} for Shanghai. We selected the city-specific optimal lags for each meteorological available by screening 1–14 days and choosing the lag that maximized variance explained in the GAM for Beijing and Shanghai, respectively. These differences reflect local climate and reporting dynamics rather than being hard-coded into the prediction model. Tables I and II show the analysis results, where the lagged average temperature, relative humidity, $PM_{2.5}$, and PM_{10} all had significant effects on daily counts of COVID-19 in both Beijing and Shanghai (p-value $<$ 2e-16). However, compared to the average temperature and relative humidity, the contributions of $PM_{2.5}$, and PM_{10} are not as great as the former two variables. Collinearity diagnostics indicated severe redundancy between $PM_{2.5}$ and PM_{10}, with Spearman values at round 0.93 and concurvity greater than 0.9. Therefore, we retain average temperature and relative humidity to modulate the transmission rate, which can yield comparable predictive skills with greater parsimony. According to the results exhibited in Fig. 2 and 3, temperature exhibited a nonlinear relationship with COVID-19 transmission. In both Beijing and Shanghai, temperatures between 13 °C and 15 °C, and 17 °C and 21 °C were associated with two small increases in COVID-19 cases. However, when the temperature was around 13 °C–17 °C, the daily counts of COVID-19 in Shanghai showed a decrease trend with the increase in temperature, while when the average temperatures were between 9 °C and 13 °C, and 17 °C and 19 °C, the COVID-19 cases in Shanghai showed an upward trend. The difference between the development trends in these two cities was caused by various reasons, including the different meteorological conditions in these two cities. As for relative humidity, its impact on COVID-19 case trends appeared more stable in Beijing. When under drier conditions (low relative humidity), COVID-19 cases tend to be higher, while more humid days see reduced transmission. However, in Shanghai, it exhibited greater variability. Since Beijing and Shanghai have distinct climates. Specifically, Shanghai has a humid subtropical climate, which experiences higher relative humidity throughout the year, while Beijing tends to have lower relative humidity compared to Shanghai. Essentially, in Shanghai's already humid environment, extremely high relative humidity may not confer additional protection and might even coincide with higher case counts. Air pollution ($PM_{2.5}$ and PM_{10}) shows similar detrimental associations with COVID-19 in both cities, but there are differences in effect magnitude and linearity. Both Shanghai and Beijing experienced higher COVID-19 case counts following days of elevated particulate matter, indicating that pollution likely exacerbates transmission or susceptibility. However, Shanghai's pollution effect appears somewhat stronger on a per-unit basis. Given a 10 $\mu g/m^3$ increase in $PM_{2.5}$ or PM_{10}, Shanghai tended to see a relatively larger percentage increase in cases than Beijing (based on the shapes of their GAM curves). This could be because Shanghai's baseline pollution is lower; therefore, an increase from clean to moderately polluted air in Shanghai might trigger a noticeable jump in cases, whereas Beijing often has a persistently higher pollution baseline, so equivalent fluctuations are less dramatic in proportion. These findings highlight the differing air pollution profiles between the two cities and their potential influence on COVID-19 transmission dynamics.

TABLE I
Hypothesis Test Results Between Smoothed Variable and Covid-19 Daily Cases in Beijing Using GAM

Smoothed Variable	EDF	Ref. df	p-Value	Deviance (%)	R^2 Adjusted
S(lag_temp)	8.962	8.999	<2e-16	42.24	0.447
S(lag_RH)	8.957	8.999	<2e-16	19.06	0.223
S(lag_PM10)	8.850	8.986	<2e-16	10.46	0.186
S(lag_PM2.5)	8.664	8.953	<2e-16	13.17	0.204

TABLE II
Hypothesis Test Results Between Smoothed Variable and Covid-19 Daily Cases in Shanghai Using GAM

Smoothed Variable	EDF	Ref. df	p-Value	Deviance (%)	R^2 Adjusted
S(lag_temp)	8.997	9.000	<2e-16	24.15	0.260
S(lag_RH)	8.996	9.000	<2e-16	16.92	0.157
S(lag_PM10)	8.998	9.000	<2e-16	16.30	0.175
S(lag_PM2.5)	8.992	9.000	<2e-16	12.93	0.140

B. Spatial Analysis of COVID-19 Epidemics in Beijing and Shanghai

In this study, we used the data of the COVID-19 epidemic in Shanghai from 5 March to 31 May 2022 and Beijing from 22 April to 30 June 2022 to conduct the analysis and prediction. The modified SEIR method is used as the primary method, and the coefficients for the epidemics in different locations are obtained through the inverse coefficient method to generate location-specific prediction results. It is important to note that the values of these coefficients vary across models, reflecting the differences in how COVID-19 progresses in each region.

Shanghai and Beijing, as two megacities in China, with the number of the confirmed cases in each district not equally distributed due to the inhomogeneity of the population density and human mobility, and so on. After the analysis, we found that Chaoyang and Pudong districts in Beijing and Shanghai both had the highest number of confirmed cases among all the districts. The primary reason for the highest ranking is

Authorized licensed use limited to: Lanzhou University. Downloaded on November 10,2026 at 10:13:19 UTC from IEEE Xplore. Restrictions apply.

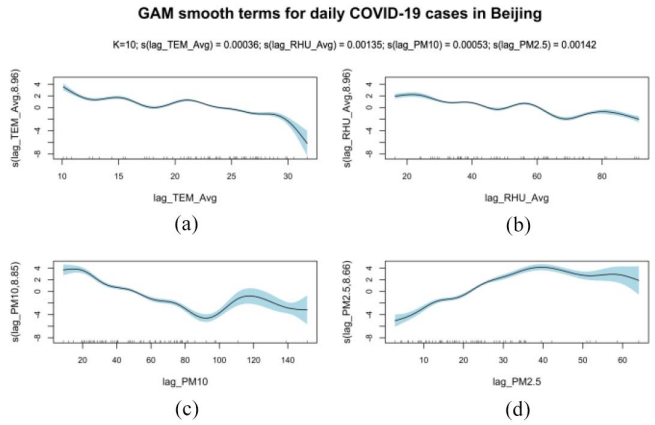


Fig. 2. GAM analysis result for Beijing. This figure shows smooth terms for the effect of lagged temperature (lag_TEM_avg), relative humidity (lag_RHU_avg), PM10 (lag_PM10), and PM2.5 (lag_PM2.5) on the response (COVID-19 cases) in Beijing, using a GAM. Each subplot represents the estimated smooth effect for one environmental variable, where the x-axis corresponds to the lag days, and the y-axis represents the estimated smooth function of each lagged variable on the response variable. (a) Effect of lagged temperature (lag_TEM_avg) on the response. (b) Effect of lagged relative humidity (lag_RHU_avg) on the response. (c) Effect of lagged PM10 (lag_PM10) on the response. (d) Effect of lagged PM2.5 (lag_PM2.5) on the response. The smoothing spans, basis dimensions for K are noted on top of the plot.

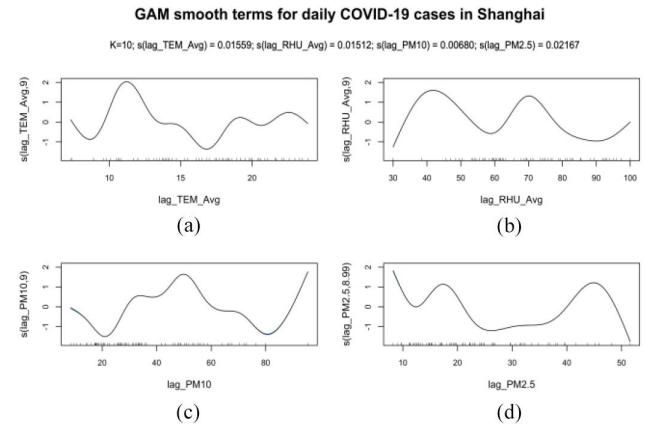


Fig. 3. GAM analysis result for Shanghai. This figure shows smooth terms for the effect of lagged temperature (lag_TEM_avg), relative humidity (lag_RHU_avg), PM10 (lag_PM10), and PM2.5 (lag_PM2.5) on the response (COVID-19 cases) in Shanghai, using a GAM. Each subplot represents the estimated smooth effect for one environmental variable, where the x-axis corresponds to the lag days and the y-axis represents the estimated smooth function of each lagged variable on the response variable. (a) Effect of lagged temperature (lag_TEM_avg) on the response. (b) Effect of lagged relative humidity (lag_RHU_avg) on the response. (c) Effect of lagged PM10 (lag_PM10) on the response. (d) Effect of lagged PM2.5 (lag_PM2.5) on the response. The smoothing spans, basis dimensions for K are noted on top of the plot.

their large population. We then further analyzed the correlation between the population and proportion of confirmed cases, and the Pearson correlation coefficients of Shanghai and Beijing are 0.85 and 0.66, respectively, which suggests that there is a strong positive correlation between these two factors. In other words, the district with a larger population indeed tends to have more

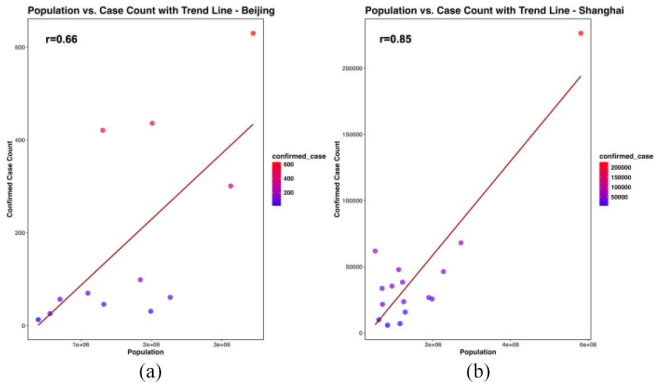


Fig. 4. Comparison of population and confirmed case in Beijing and Shanghai: The plot shows the relationship between population size and confirmed case counts for (a) Beijing and (b) Shanghai. Each data point represents a different district, with the color gradient indicating the confirmed case count. A trend line is fitted to each dataset, showing the general increasing trend in case count with population size. The Pearson correlations for Beijing and Shanghai are 0.66 and 0.85, respectively.

confirmed cases (shown in Fig. 4(a) and (b)). However, there are some exceptions such as Fangshan and Huangpu districts, where the population is smaller but the number of confirmed cases is larger than in other districts. In order to explain this phenomenon, we conducted spatial analysis on the distribution of the confirmed cases in these two cities. Since an outbreak of an epidemic always shows spatial clustering features, the spread of an epidemic is affected by many external factors, such as population size, human mobility, and medical level. To figure out whether the distributions of COVID-19 epidemics in Beijing and Shanghai also follow such patterns, we applied the spatial-weighted K-means method to examine the spatial clustering feature in these two cities. According to the analysis results (shown in Fig. 5 and 6), we found that Beijing had three distinct clusters in terms of the distribution of COVID-19, and we labeled them as High risk, Medium risk, and Low risk areas, while Shanghai had five distinct clusters, labeling them as High risk, Medium High risk, Medium risk, Medium Low risk, and Low risk areas. This spatial clustering feature explains why districts like Fangshan and Huangpu also had higher records of daily cases, as the spatial clustering shows that such districts are closer to the hotspot regions, thus having a greater tendency to be affected.

C. Prediction Results for Shanghai and Beijing

Based on the feature of the distribution of the confirmed cases, we used the MDEP method to perform a retrospective forecast on the development of the COVID-19 epidemic in Shanghai and Beijing. As mentioned in the method section, we conducted the prediction process spatially. The results from Fig. 7, where the blue dotted lines represent the real values, while the red dotted lines represent the predicted values of different risk level regions in Shanghai and Beijing, respectively. Moreover, the blue and red solid lines represent the overall trends of real values and predicted results. According to this figure, we can conclude that the MDEP method can

Authorized licensed use limited to: Lanzhou University. Downloaded on November 10,2026 at 10:13:19 UTC from IEEE Xplore. Restrictions apply.

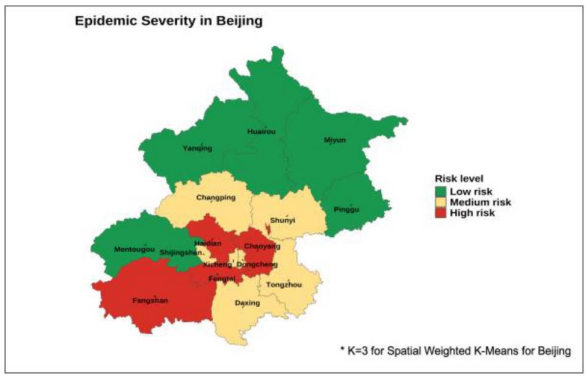


Fig. 5. Epidemic severity in Beijing: The map visualizes the epidemic severity across different districts in Beijing, categorized by risk levels. Areas with high risk are shown in red, medium risk areas in yellow, and low risk areas in green, providing a spatial overview of epidemic trends within the city.

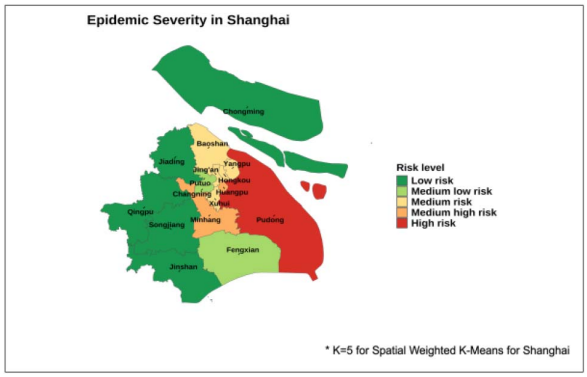


Fig. 6. Epidemic severity in Shanghai: The map visualizes the epidemic severity across different districts in Shanghai, categorized by risk levels. Areas with high risk are shown in red, medium high risk areas in brown, medium risk areas in yellow, medium low risk areas in light green, and low risk areas in green, providing a spatial overview of epidemic trends within the city.

capture the development trends well in general, which could be proved by the values of MAE, RMSE, and R^2. However, when there were some sudden surges occurring in a short period of time, the MDEP method cannot depict such trend precisely. For example, the MDEP method failed to reflect the two sudden surges that occurred during April in low-risk area in Shanghai. Moreover, the accuracy of prediction results will be lower due to the fluctuations in the number of confirmed the cases are more frequent and larger over a short period of time. This situation might be caused by several reasons, one of them may be the delayed report, so counts that occurred over several days are posted on a single date. Another possible reason could be delayed tests, which means some people might not take the test in the first place, even though they have symptoms onset. This phenomenon can be observed in all risk areas in both Shanghai and Beijing, where the frequent fluctuations occurred during the progress of the COVID-19 epidemics, especially in the medium and low risk areas in Beijing, where the jumps of the daily cases are large and frequent. Despite the relatively small scale of confirmed cases in these areas, the magnitude of change

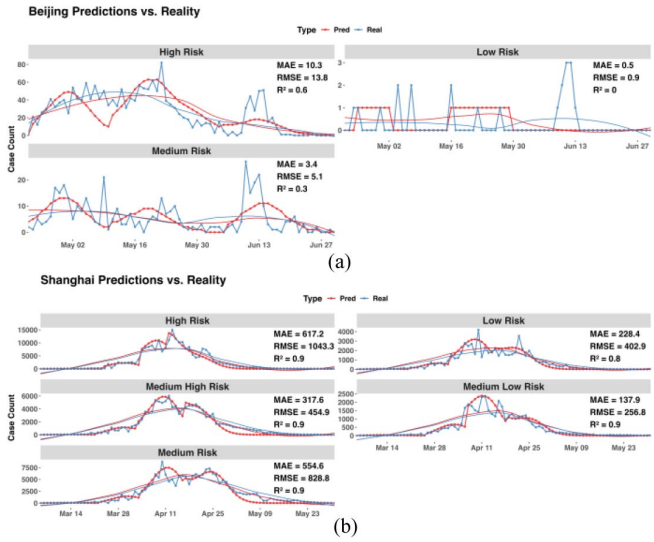


Fig. 7. Prediction results and actual values for Beijing and Shanghai: The figure presents the predicted and actual epidemic case counts for districts of different risk levels in (a) Beijing and (b) Shanghai. The model's prediction accuracy is assessed with statistical measures such as MAE, RMSE, and R^2 for each risk category.

was substantial. Consequently, the MDEP method was unable to accurately forecast this dramatic rise, resulting in lower prediction accuracy for such districts, with the values of R^2 in low and medium risk areas being 0 and 0.29, respectively. This pattern underscores the challenge posed by rapid and significant changes in epidemic dynamics to the predictive reliability of the model, highlighting an area for potential refinement in forecasting methodologies for infectious diseases.

D. Model Validation Results

After obtaining the prediction results in each risk area, we applied the TEP method and summed these results to get the integrated prediction results for Shanghai and Beijing and compared the prediction results of Shanghai and Beijing generated by the MDEP method and the modified SEIR model. It should be noted that the MDEP method and modified SEIR model were conducted on city level. As shown in Fig. 8, we evaluate the 95% PI results for the three models, namely TEP, MDEP, and modified SEIR, on daily and cumulative cases in Beijing and Shanghai. For cumulative counts, the TEP and MDEP medians closely follow the observed trajectories in both cities, with PIs that remain relatively tight and attain near nominal coverage. By contrast, the modified SEIR median plateaus too early and underestimate the final size, and their wider ribbons indicate poorer sharpness and structural mismatch. For daily counts, TEP and MDEP reproduce the timing and amplitude of waves more faithfully, with uncertainty widening around the peaks as expected. However, the modified SEIR median misses parts of the multipeak structure and requires substantially broader PIs to maintain coverage. Across cities, Shanghai shows larger variability and higher case counts, reflected in correspondingly wider daily and cumulative PIs for all methods. Overall, TEP provides calibrated PIs with better sharpness than the modified

Authorized licensed use limited to: Lanzhou University. Downloaded on November 10,2026 at 10:13:19 UTC from IEEE Xplore. Restrictions apply.

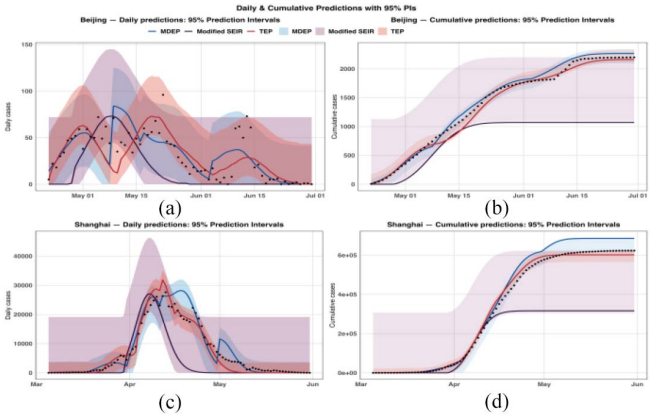


Fig. 8. Comparison between predicted daily and cumulative COVID-19 cases and reality in Beijing and Shanghai: This plot compares the predicted and actual daily and cumulative COVID-19 case counts for (a, b) Beijing and (c, d) Shanghai, where the red, blue, and purple lines represent the TEP method, MDEP method, and modified SEIR model, respectively, and the black points represent the real values. The shaded bands denote 95% prediction intervals for each method/model.

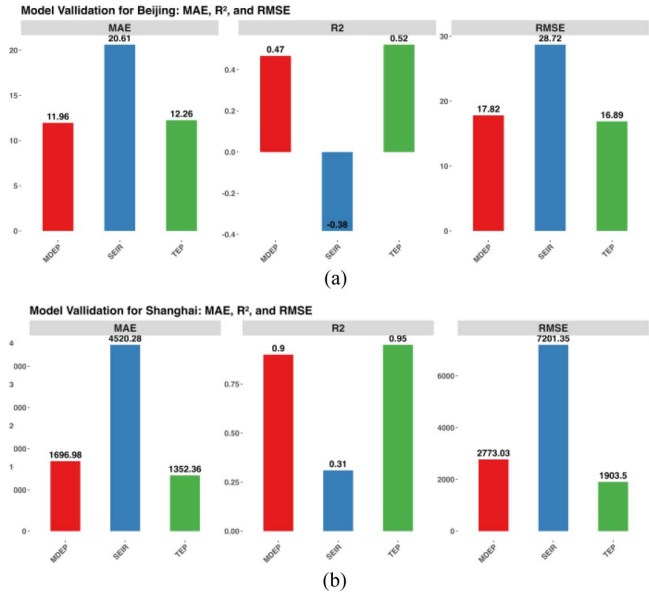


Fig. 9. Validation of epidemic methods in Beijing and Shanghai: This figure compares the MAE, R^2, and RMSE values for three epidemic prediction methods (MDEP, SEIR, and TEP) for (a) Beijing and (b) Shanghai. The bar graphs show the MAE, R^2, and RMSE for each model, with the MAE and RMSE values reflecting prediction errors, and the R^2 values indicating the strength of the model fit.

SEIR, and performance is slightly better than MDEP near the growth and waning faces, which supports its use for operational prediction with quantified uncertainty. Moreover, the comparative results indicate that the integrated prediction results in terms of the daily new cases (shown as the red lines), which were generated by the TEP method, can depict the real development trend of the COVID-19 epidemic better than the MDEP method (blue lines) and modified SEIR method (green lines) can. Especially during the period between April and May, when the COVID-19 epidemic had developed to the peak stage, and the TEP method exhibits a more similar trend to the real trend than the MDEP and modified SEIR method does. However, the TEP method exhibits a better performance in predicting the development of the COVID-19 epidemic in Shanghai than in Beijing. Since the development trend of COVID-19 in Shanghai was more stable, which means there were fewer sudden surges. In addition, we conducted a validation analysis on these methods, and the results are shown in Fig. 9. According to this figure, we can observe that the TEP method could generate more accurate results than MDEP and modified SEIR methods do, as the values of MAE and RMSE of the TEP method are smaller than those of the other two methods, and this is particularly true in Shanghai. While the MAE of the TEP method is a little bit higher than that of the MDEP method in Beijing, the other two metrics of the TEP method both show a better performance than the MDEP method. Moreover, the accuracy rates were calculated for the predictions on cumulative cases (shown in Table III), which means that TEP has lower error rates when compared with the MDEP method in both groups. Therefore, for cities like Shanghai and Beijing, which have a massive population, the TEP method is a more suitable method to generate prediction results with higher accuracy rates.

TABLE III
COMPARISON OF THE ACCURACY RATES OF EACH METHOD

Method	Shanghai Accuracy (%)	Beijing Accuracy (%)
TEP	84.83	94.27
MDEP	67.83	91.91
Modified SEIR	45.06	52.53

E. Discussion

The rapid advancement of society and technology has not only significantly enhanced daily living but also presents challenges, notably the increasing frequency of infectious disease outbreaks. Environmental factors play a vital role in terms of triggering the outbreaks and spread of infectious diseases. The global impact of COVID-19 has particularly underscored this issue, catalyzing heightened contributions made by environmental variables. Researches pointed out extreme weather events, such as heat and cold waves and the outbreak of floods, will amplify the negative impacts of COVID-19, including accelerating the increase of COVID-19 cases [44], [45], [46]. In addition, research efforts toward accurately predicting epidemics like COVID-19 are of great importance. Despite the widespread use of predictive models, accurately forecasting the progression of infectious diseases remains a significant challenge. To address this, our study employed a GAM to quantify the impact of environmental factors on disease transmission and introduced the TEP method to overcome limitations of existing forecasting approaches by integrating both temporal and spatial dynamics.

The TEP method presents a significant advancement in epidemiological forecasting by employing an ensemble forecast technique. This approach effectively mitigates prediction errors associated with the incompleteness of initial values [47], a common challenge in the early stages of an epidemic when

Authorized licensed use limited to: Lanzhou University. Downloaded on November 10,2026 at 10:13:19 UTC from IEEE Xplore. Restrictions apply.

daily new case numbers often fail to accurately reflect the true trajectory of the disease. In that case, if we use these initial values to predict the future development of the epidemic, the results we obtained will highly likely underestimate the real trend. In addition, human mobility in big cities such as Shanghai also plays an important role in affecting the development of the epidemic. Classic epidemiological models typically do not account for the complexities of human mobility, leading to inaccuracies in simulating the multiwave nature of epidemics. While the TEP method does not directly incorporate human mobility models, it enhances prediction accuracy by temporally and spatially integrating results, as human mobility data are often difficult to obtain, especially for timely predictions during the early stages of an epidemic. Moreover, compartmental dynamics fitted at the risk level absorb the net effects of short-range mixing such as human mobility patterns embedded in daily case counts. The TEP method integrates waves within each risk-level region and then aggregates across regions, thereby approximating the diffusion of infection pressure from hotspot to neighboring areas. In our case study, the TEP method outperformed the modified SEIR and the time-only MDEP for daily and cumulative prediction, which indicates that special integration provides additional predictive value even without explicit mobility data. This feature enables the depiction of the multiwave trend of an epidemic, offering a practical balance between timeliness and accuracy. The TEP method is particularly applicable when 1) special units are small enough, the incidence is heterogeneous spatially autocorrelated, for example, the clusters are identifiable through spatial analysis. Therefore, they bring trans-carry predictive information; and 2) routine intra-urban mobility remains relatively stable over the prediction horizon, which allows its influence to be captured in district case trajectories even without explicit ability data. Under these conditions, district-wise two-way ensemble followed by spatial aggregation provides a practical proxy for population movement and yields the best city-level prediction without minimal data requirements, making it particularly suitable for governments or regions seeking rapid prediction with constrained data resources. Although the exclusion of human mobility models in TEP may result in less precision compared to more complex models, its requirement for only epidemic-related data streamlines the prediction process, offering a practical balance between timeliness and accuracy.

Despite the advantages of the TEP method, some of the flaws of this method should not be neglected. During low incidence periods, discrete transmission and reporting processes can cause volatility that deterministic ordinary differential equations (ODEs) may not capture. Therefore, stochastic compartmental and state-space formulations, such as CTMC SEIR with Gillespie simulation or an SDE model with mean-reverting transmission rate, that respect discrete events and parameter availability are recommended [48], [49]. In reality, the number of cases of an epidemic could be small and follow a discrete Poisson distribution, when the ordinary differential equations are not suitable for solving such kinds of situations. Moreover, the GAM analysis results indicated that some external factors such as control policy and human gatherings should also be considered to establish a more sophisticated model to provide better prediction performance. Therefore, we will incorporate these stochastic models into the TEP work frame to improve the predictive performance of our model on discrete and low count scenarios.

IV. Conclusion

In contexts where epidemic data are collected accurately and promptly, the TEP method demonstrates its potential to produce reliable forecasts, thereby facilitating efficient resource allocation and decision-making for governmental departments. This balance of expedience and precision underscores the utility of TEP as a valuable tool in epidemic modeling, especially in scenarios where rapid response and resource optimization are critical. The TEP method enhances prediction accuracy by integrating and refining outputs from the existing MDEP framework. Through this integrative approach, the TEP method effectively serves as a calibration mechanism for MDEP, harmonizing its separate outputs to yield more precise predictions. Comparative analysis of predictions from both MDEP and TEP methods demonstrate the latter's superior accuracy in forecasting disease progression, underscoring its potential as a significant advancement in the field of epidemic modeling. This article details the methodology underpinning the TEP method, its comparative advantages over the MDEP method, and the implications of these findings for future epidemic prediction and management. The integration of advanced modeling techniques in TEP represents an important step towards more reliable and accurate epidemic forecasting, a crucial tool in the ongoing battle against infectious diseases.

References

[1] H. Heesterbeek et al., "Modeling infectious disease dynamics in the complex landscape of global health," *Science*, vol. 347, no. 6227, 2015, Art. No. aaa4339.
[2] K. Rock, S. Brand, J. Moir, and M. Keeling, "Dynamics of infectious diseases," *Rep. Prog. Phys.*, vol. 77, no. 2, 2014, Art. No. 026602.
[3] S. Gandon, T. Day, C. J. E. Metcalf, and B. T. Grenfell, "Forecasting epidemiological and evolutionary dynamics of infectious diseases," *Trends Ecol. Evol.*, vol. 31, no. 10, pp. 776–788, 2016.
[4] J. Huang et al., "Global prediction system for COVID-19 pandemic," *Sci. Bull.*, vol. 65, no. 22, pp. 1884–1887, 2020.
[5] J. Huang et al., "Development of the second version of global prediction system for epidemiological pandemic," *Fundam. Res.*, vol. 4, no. 3, pp. 516–526, 2024.
[6] L. Zhang et al., "Optimal parameterization of COVID-19 epidemic models," *Atmos. Ocean. Sci. Lett.*, vol. 14, no. 4, 2021, Art. No. 100024.
[7] H. G. Hong and Y. Li, "Estimation of time-varying reproduction numbers underlying epidemiological processes: A new statistical tool for the COVID-19 pandemic," *PLoS One*, vol. 15, no. 7, 2020, Art. No. e0236464.
[8] C. You et al., "Estimation of the time-varying reproduction number of COVID-19 outbreak in China," *Int. J. Hyg. Environ. Health*, vol. 228, 2020, Art. No. 113555.
[9] I. Cooper, A. Mondal, and C. G. Antonopoulos, "A SIR model assumption for the spread of COVID-19 in different communities," *Chaos Solitons Fractals*, vol. 139, 2020, Art. No. 110057.
[10] P. Singh and A. Gupta, "Generalized SIR (GSIR) epidemic model: An improved framework for the predictive monitoring of COVID-19 pandemic," *ISA Trans.*, vol. 124, pp. 31–40, 2022.
[11] S. Altizer, R. S. Ostfeld, P. T. Johnson, S. Kutz, and C. D. Harvell, "Climate change and infectious diseases: From evidence to a predictive framework," *Science*, vol. 341, no. 6145, pp. 514–519, 2013.

Authorized licensed use limited to: Lanzhou University. Downloaded on November 10,2026 at 10:13:19 UTC from IEEE Xplore. Restrictions apply.

[12] P. R. Epstein, "Climate change and emerging infectious diseases," *Microbes Infect.*, vol. 3, no. 9, pp. 747–754, 2001.
[13] X. Wu, H. Tian, S. Zhou, L. Chen, and B. Xu, "Impact of global change on transmission of human infectious diseases," *Sci. China Earth Sci.*, vol. 57, pp. 189–203, Feb. 2014.
[14] M. E. Martinez, "The calendar of epidemics: Seasonal cycles of infectious diseases," *PLoS Pathog.*, vol. 14, no. 11, 2018, Art. No. e1007327.
[15] X. Liu et al., "The role of seasonality in the spread of COVID-19 pandemic," *Environ. Res.*, vol. 195, 2021, Art. No. 110874.
[16] Z. Huang et al., "Optimal temperature zone for the dispersal of COVID-19," *Sci. Total Environ.*, vol. 736, 2020, Art. No. 139487.
[17] M. Marquès and J. L. Domingo, "Positive association between outdoor air pollution and the incidence and severity of COVID-19," *Environ. Res.*, vol. 203, 2022, Art. No. 111930.
[18] E. Conticini, B. Frediani, and D. Caro, "Can atmospheric pollution be considered a co-factor in extremely high level of SARS-CoV-2 lethality in Northern Italy?" *Environ. Pollut.*, vol. 261, 2020, Art. No. 114465.
[19] N. Van Doremalen et al., "Aerosol and surface stability of SARS-CoV-2 as compared with SARS-CoV-1," *N. Engl. J. Med.*, vol. 382, no. 16, pp. 1564–1567, 2020.
[20] M. Zhang et al., "Human mobility and COVID-19 transmission: A systematic review and future directions," *Ann. GIS*, vol. 28, no. 4, pp. 501–514, 2022.
[21] T. Hu et al., "Human mobility data in the COVID-19 pandemic: Characteristics, applications, and challenges," *Int. J. Digit. Earth*, vol. 14, no. 9, pp. 1126–1147, 2021.
[22] H. Li et al., "Impact of human mobility on the epidemic spread during holidays," *Infect. Dis. Model.*, vol. 8, no. 4, pp. 1108–1116, 2023.
[23] M. H. Schoot Uiterkamp et al., "The role of inter-regional mobility in forecasting SARS-CoV-2 transmission," *J. R. Soc. Interface*, vol. 19, no. 193, 2022, Art. No. 20220486.
[24] M. Chinazzi et al., "The effect of travel restrictions on the spread of the 2019 novel coronavirus (COVID-19) outbreak," *Science*, vol. 368, no. 6489, pp. 395–400, 2020.
[25] A. Findlater and I. I. Bogoch, "Human mobility and the global spread of infectious diseases: a focus on air travel," *Trends Parasitol.*, vol. 34, no. 9, pp. 772–783, 2018.
[26] A. J. Tatem, D. J. Rogers, and S. I. Hay, "Global transport networks and infectious disease spread," *Adv. Parasitol.*, vol. 62, pp. 293–343, 2006.
[27] S. T. Stoddard et al., "The role of human movement in the transmission of vector-borne pathogens," *PLoS Negl. Trop. Dis.*, vol. 3, no. 7, 2009, Art No. e481.
[28] A. Wesolowski et al., "Quantifying the impact of human mobility on malaria," *Science*, vol. 338, no. 6104, pp. 267–270, 2012.
[29] S. Riley, "Large-scale spatial-transmission models of infectious disease," *Science*, vol. 316, no. 5829, pp. 1298–1301, 2007.
[30] L. Alessandretti, "What human mobility data tell us about COVID-19 spread," *Nat. Rev. Phys.*, vol. 4, no. 1, pp. 12–13, 2022.
[31] H. Fang, L. Wang, and Y. Yang, "Human mobility restrictions and the spread of the novel coronavirus (2019-nCoV) in China," *J. Public Econ.*, vol. 191, 2020, Art. No. 104272.
[32] M. U. Kraemer et al., "The effect of human mobility and control measures on the COVID-19 epidemic in China," *Science*, vol. 368, no. 6490, pp. 493–497, 2020.
[33] J. Huang et al., "Multi-source dynamic ensemble prediction of infectious disease and application in COVID-19 case," *J. Thorac. Dis.*, vol. 15, no. 7, pp. 4040–4052, 2023.
[34] J. Ma et al., "Skillful seasonal predictions of continental East-Asian summer rainfall by integrating its spatio-temporal evolution," *Nat. Commun.*, vol. 16, 2025, Art No. 273.
[35] J. Ma et al., "Skillful seasonal forecasting of spatiotemporal rainfall anomalies over High Mountain Asia," *Geophys. Res. Lett.*, vol. 52, no. 14, 2025, Art No. e2025GL117001.
[36] B. Cheng et al., "Influence of weather and air pollution on concentration change of PM2.5 using a generalized additive model and gradient boosting machine," *Atmos. Environ.*, vol. 255, 2021, Art. No. 118437.
[37] R. D. Peng, F. Dominici, and T. A. Louis, "Model choice in time series studies of air pollution and mortality," *J. R. Stat. Soc. Ser. A Stat. Soc.*, vol. 169, no. 2, pp. 179–203, 2006.
[38] J. Wang and X. Su, "An improved K-means clustering algorithm," in *Proc. 2011 IEEE 3rd Int. Conf. Commun. Softw. Netw.*, 2011, pp. 44–46.
[39] H. Yamada, "Moran's I for multivariate spatial data," *Mathematics*, vol. 12, no. 17, 2024, Art. No. 2746.
[40] Y. Zhu, "Ensemble forecast: A new approach to uncertainty and predictability," *Adv. Atmos. Sci.*, vol. 22, pp. 781–788, 2005.
[41] E. Cheynet, *Generalized SEIR epidemic model (fitting and computation)*," Github, 2020. [Online]. Available: https://github.com/ECheynet/SEIR/releases/tag/v4.8.4
[42] L. Peng, W. Yang, D. Zhang, C. Zhuge, and L. Hong, "Epidemic analysis of COVID-19 in China by dynamical modeling," 2021, *arXiv:2002.06563*.
[43] C. Lung-Chang, L.-W. Antony Chen, and R.-T. Lin, "Lagged meteorological impacts on COVID-19 incidence among high-risk counties in the United States—A spatiotemporal analysis," *J. Exposure Sci. Environ. Epideniol.*, vol. 32, no. 5, pp. 774–781, 2022.
[44] X. Lian et al., "Cold waves accelerate the spread of infectious diseases," *Geophys. Res. Lett.*, vol. 51, no. 15, 2024, Art. No. e2024GL109405.
[45] X. Lian et al., "Heat waves accelerate the spread of infectious diseases," *Environ. Res.*, vol. 231, 2023, Art. No. 116090.
[46] J. Huang et al., "Water transmission increases the intensity of COVID-19 outbreaks," *Front. Public Health*, vol. 10, 2022, Art. No. 808523.
[47] T. N. Palmer, et al., "Ensemble prediction," in *Proc. ECMWF Seminar Validation Models Over*, vol. 1. Europe, Reading, U.K.: ECMWF, 1993, pp. 21–66.
[48] M. J. Keeling and P. Rohani, *Modeling Infectious Diseases in Humans and Animals.* Princeton, NJ, USA: Princeton Univ. Press, 2008.
[49] O. N. Bjørnstad, *Epidemics. Models and Data Using R.* Cham, Switzerland: Springer, 2018.



Yingjie Zhao received the B.S. degree in engineering mechanics from Lanzhou University of Technology, Lanzhou, China, in 2016, the M.S. degree in applied statistics from the University of Wollongong, Wollongong, NSW, Australia, in 2019. She is currently working toward the Ph.D. degree in climatology with Lanzhou University, Lanzhou.

From 2018 to 2019, she was an Intern Algorithm Engineer with Beijing Chen'an Technology Company, Ltd., Beijing, China. From 2019 to 2020, she was an intern Data Analyst with LEFTA Company, Sydney, Australia. From 2020 to 2022, she was a Research Assistant with Western Ecological Security Collaborative Innovation Center, Lanzhou University.

Her research interests include modelling of infectious diseases and environmental health.



Jianping Huang received the double B.S. degrees in atmospheric detection and synoptic dynamics from Nanjing University of Information Science and Technology, Nanjing, China, in 1982, the M.S. degree in meteorology from Northwest Institute of Eco-Environment and Resources, Chinese Academy of Sciences, Lanzhou, China, in 1986, and the Ph.D. degree in synoptic dynamics from Lanzhou University, Lanzhou, in 1988.

He is a Distinguished Professor with the College of Atmospheric Sciences and the Director of the Collaborative Innovation Center for Western Ecological Safety, Lanzhou University. He is currently an Academician with Chinese Academy of Sciences and a Fellow of the World Academy of Science.

His research interests include climate change, dryland climate, dust aerosol, carbon cycle, and oxygen cycle.



Rui Wang received the B.S. degree in preventive medicine and the M.S. degree in epidemiology and health statistics from Kunming Medical University, Kunming, China, in 2018 and 2021, respectively. She is currently working toward the Ph.D. degree in climatology with Lanzhou University, Lanzhou, China.

From 2021 to 2022, she was a Research Assistant with Western Ecological Security Collaborative Innovation Center, Lanzhou University. Her research interests include epidemiological forecasting, environment, and health fields.

Authorized licensed use limited to: Lanzhou University. Downloaded on November 10,2026 at 10:13:19 UTC from IEEE Xplore. Restrictions apply.



Han Li received the B.S. degree in atmospheric sciences from Lanzhou University, Lanzhou, China, in 2023. She is currently working toward the Ph.D. degree in climatology with Lanzhou University.

Her research interests include prediction research on the impact of meteorological and environmental factors on infectious diseases.



Wei Yan received the B.S. degree in atmospheric science from Lanzhou University, Lanzhou, China, in 2022. He is currently working towards the Ph.D. degree in climatology from Lanzhou University.

His research interests include epidemic prediction and construction of epidemic systems.



Xinbo Lian received the B.S. degree in environmental engineering and the M.S. degree in environmental science and engineering from Nanjing University of Information Science and Technology, Nanjing, Jiangsu, China, in 2016 and 2019, respectively, and the Ph.D. degree in climatology from Lanzhou University, Lanzhou, China, in 2023.

She is currently a Postdoctoral Researcher with the Geography Postdoctoral Research Station, Lanzhou University. Her research interests include climate change and human health, epidemic attribution analysis, and environmental impact effects.



Zihan Hao received the M.S. degree in applied statistics from Lanzhou University, Lanzhou, China in 2022. She is currently working toward the Ph.D. degree in meteorology with Lanzhou University.

Her research interests include data assimilation and environmental health.

Authorized licensed use limited to: Lanzhou University. Downloaded on November 10,2026 at 10:13:19 UTC from IEEE Xplore. Restrictions apply.